THE EFFECT OF ELECTRODE SURFACE TOPOGRAPHY ON THE STRUCTURE AND DIFFERENTIAL CAPACITANCE OF THE ELECTRIC DOUBLE LAYER CAPACITOR

by

Liulei Cao

A thesis submitted to the faculty of
The University of Utah
in partial fulfillment of the requirements for the degree of

Master of Science

Department of Materials Science and Engineering

The University of Utah

August 2011

The University of Utah Graduate School

STATEMENT OF THESIS APPROVAL

The thesis of **Liulei Cao**

has been approved by the following supervisory committee members:

Grant D. Smith	, Chair	**05/19/2011** Date Approved
Anil V. Virkar	, Member	**05/19/2011** Date Approved
Ashutosh Tiwari	, Member	**05/19/2011** Date Approved

and by **Anil V. Virkar** , Chair of the Department of **Materials Science and Engineering**

and by Charles A. Wight, Dean of The Graduate School.

ABSTRACT

Molecular dynamics simulations were conducted to study the structure and differential capacitance of the electric double layer capacitor by varying electrode topography. Studying the dependence of structure and differential capacitance (DC) on electrode potential is a central point of electric double layer (EDL) models, from the early Gouy-Chapman approximation to the more recent Kornyshev formulation or Lamperski treatment. Although the influence on DC of temperature, density, polarisability and dispersion interactions of room temperature ionic liquid (RTIL) electrolyte is becoming more understood, the effect of electrode topography on DC remains unclear and perhaps controversial. Moreover, the variability of DC results for poorly prepared polycrystalline electrodes may indicate a strong dependence of EDL structure and DC on the topography of electrode surface.

In this work, we employ molecular dynamics simulations to prove that the crystallographic orientation and the surface roughness of electrode could intensely alter the shape of DC curve as a function of electrode potential, especially near the potential of zero charge (PZC). Specifically, we simulated a RTIL electrolyte, consisting of 1-ethyl-3-methyl imidazolium ($EMIM^+$), bis-fluorosulfonyl imide (FSI^-), and Li+ (in a molar ratio of 24:31:7), in contact with two types of graphite electrodes: one is graphite with atomically flat basal plane

and the other is graphite with edge orientation.

This work demonstrates that the capacitor with atomically flat basal plan graphite generates a camel-shaped DC curve; while, the capacitor with edge orientation graphite engenders a bell-shaped DC curve. Furthermore, the capacitor with edge orientation graphite displays a significantly larger DC (almost double) than the capacitor with atomically flat basal plane graphite near PZC. Additionally, these findings coincide with the results of numerous recent experiments. Thus, we conclude that the crystallographic orientation and surface roughness will modify the EDL structure and hence, vary the DC curve of the EDLC.

TABLE OF CONTENTS

LIST OF FIGURES

ACKNOWLEDGEMENTS

I acknowledge my special indebtedness and express my deep appreciation to my research advisor, Dr. Grant Smith. I also would like to express my very sincere thanks Dr. Jenel Vatamanu, Dr. Oleg Borodin and Dr. Dmitry Bedrov for their excellent suggestions and valuable discussions. I thank all my fellow researchers for their assistance and support in carrying on this research.

CHAPTER 1

INTRODUCTION

1.1 Electric double-layer capacitor

A capacitor is an electronic component that stores energy in the form of an electrostatic field. Basically, a capacitor is made up of a pair of conductors separated by a dielectric. When there is a potential difference (voltage) across the conductors, a static electric field develops in the dielectric that stores energy in the field. Usually, electrical energy can be stored in two fundamental ways: capacitors and batteries. Batteries, which depend on Faradaic oxidation and reduction of charge carriers in electrolyte, have relatively slow charge and discharge rates. Capacitors, on the other hand, can be charged and discharged much faster than batteries, since no chemical reactions are involved during the process. In other words, capacitors possess higher power density than batteries. An electric double-layer capacitor (EDLC), also known as super-capacitor, is an electrochemical capacitor with relatively high energy density. Compared to the energy density of conventional electrolytic capacitors, EDLCs' energy density is typically on the order of thousands of times greater.

1.1.1 Electrodes of electric double-layer capacitor

The requirements for electrodes of EDLCs are (1) long-term thermal, mechanical and electrical stability, i.e., good resistance to electrochemical oxidation and reduction; (2) high specific surface area, on the order of 10^3 m^2/g;[1] (3) good intraparticle and interparticle conductivity; (4) good electrolyte accessibility. In general, super-capacitors improve the energy density through the use of nanoporous materials. The surface area of such a material is many times greater than that of a traditional material like aluminum, allowing many more charge carriers to be stored in a unit volume or weight. Thus, carbon materials, especially in their more dispersed and conducting forms, including materials having fibrous or foam-like morphologies, are being researched intensively.

Activated charcoal is a powder made up of extremely small and very “rough” particles, and it forms a low-density heap with many holes that resemble a sponge.[2] However, activated charcoal is not the best material for EDLCs. The charge carriers are actually quite large when surrounded by solvent molecules, and are often larger than the holes in the charcoal, limiting the storage capacity of charge carriers.

Graphene is highly conductive and has excellent surface area per unit weight or volume. A specific energy density of 85.6 Wh/kg at room temperature and 136 Wh/kg at 80 ℃ has been observed at a current density of 1 A/g.[3] EDLCs usually make full utilization of high intrinsic capacitance and specific surface area of single-layer graphene by preparing curved graphene sheets that do not restack face-to-face. The curved shape enables the formation of mesopores

accessible to and wettable by ionic liquids capable of operating at a voltage larger than 4 V.[3]

Carbon nanotubes have excellent nanoporous properties, allowing spaces for the polymer to sit in the tube and act as an electrolyte.[4] Carbon nanotubes can effectively store about the same amount of charge as charcoal per unit surface area, but nanotubes can be arranged in a more ordered pattern that exposes greater surface area to electrolytes. Carbon aerogel,[5] solid activated carbon, tunable nanoporous carbon,[6] and mineral-based carbon are the other carbon-based materials used as electrodes in super-capacitors.

1.1.2 Electrolytes of electric double-layer capacitor

Two kinds of liquid electrolytes are commonly used in EDLCs, organic liquid electrolyte and ionic liquid electrolyte. Organic liquid electrolyte in super-capacitors usually consists of organic solvents, such as ethylene carbonate (EC), diethyl carbonate (DEC), and dimethyl carbonate (DMC). As electrolytes, organic liquids have numeric advantages, such as good thermal and electrical stability, high ionic conductivity, low cost, and forming stable solid-electrolyte interface (SEI). Although certain organic solvents are easy to decompose on anodes during charging, these solvents only decompose on initial charging and form a stable SEI layer, which is electrically insulating yet provides sufficient ionic conductivity. The dense and stable SEI forms at a relatively high voltage and prevents decomposition of the electrolyte after the initial charge.

Recently, ionic liquids have gained popularity as electrolytes. An ionic liquid is a salt whose melting point is below some arbitrary temperature, such as

100℃. More specifically, room temperature ionic liquids (RTILs) are ionic compounds that have melting points below 25℃ or remain as liquids at room temperature. While ordinary liquids such as water and gasoline consist predominantly of electrically neutral molecules, ILs are largely made of ions and short-lived ion pairs. There are a number of reasons that RTILs have generated intense interest over the last several years as electrolytes. These include a large workable temperature range (up to 300℃), relatively high ionic and electric conductivity, and a high degree of thermal/electrical stability. Moreover, RTILs are generally nonflammable, possess extremely low vapor pressures, and are good solvents for organic, inorganic and polymeric materials.

1.2 Structure of electric double-layer capacitor

The structure of an EDLC is a solid/electrolyte interface that appears on the surface of an electrode when it is placed into a liquid electrolyte. The electric double layer is usually most apparent in systems with a large specific surface area. Several models have already been created and developed to describe the electric double layer. In 1853, Helmholtz created the first model for the distribution of ions near the surface of a metal.[7] He envisaged two parallel layers of charges-one on a metal surface and the other on the solution side. The two sheets, each carrying opposite signs, are a few nanometers away, exactly as in the case of an EDLC.

Later Gouy and Chapman made significant improvements by considering that ions in solution are subject to thermal motion so that their distribution from the metal surface turns out diffusion.[7] They also found that near the bulk

electrolyte the electric potential is exponentially lower than it is near the electrode.[8] However, it is noted that the Gouy-Chapman model fails for highly charged electric double layers. To resolve this problem, Stern combined the Helmholtz model and the Gouy-Chapman model together, giving an internal Helmholtz layer and an external diffuse layer.[9]

In 1947, Grahame, who developed a more complex model, also considering whether an ion is solvated or interacts directly with the solid wall, transferred the knowledge of electrolyte solution structure into the model of a metal/solution interface.[10] To date, the Gouy-Chapman-Stern-Grahame model is still qualitatively accepted, although some new parameters are introduced to overcome the limitations of this model. They are reviewed in J. Lyklema's Fundamentals of Interface and Colloid Science.[11]

1.3 Differential capacitance of electric double-layer capacitor

Usually, a capacitor is characterized by a single value – capacitance, the ratio of electric charge stored on each electrode to the potential difference between them. Under normal conditions, a typical electrolytic capacitor displays capacitance in the range of tens of millifarads, whereas the capacitance of same size EDLC might reach several farads, an improvement of two orders of magnitude. Capacitance is essentially a function of overlapped surface area and separation distance of the electrodes and dielectric properties of electrolyte in between the electrodes. Normally, the capacitance is greater when there is a narrow separation between electrodes with large overlapped surface area. Differential capacitance is a measure of the voltage dependent capacitance of a

nonlinear capacitor, such as an electric double layer capacitor. It is defined as the rate of change of stored charge or surface charge divided by the rate of change of voltage between electrodes or the electric surface potential.

1.4 Application of electric double-layer capacitor

EDLCs are devices that can store electrical energy and they can be charged/discharged at a much faster rate than conventional batteries. Therefore, they have aroused interest for various applications, including electric vehicles, consumer electronics, and alternative energy.

1.4.1 Automotive

EDLCs first appeared on tanks and submarines as motor starters, and they have started to be used in diesel trucks and railroad locomotives as the cost has fallen. Since the earliest years of this century, they have attracted intense attention for regenerative braking applications and for providing a booster charge in response to sudden power demands, since their charge rate is much faster than that of traditional batteries. With EDLCs' energy densities improving, they become an attractive replacement for batteries in all-electric cars and plug-in hybrids. When used together with batteries, EDLCs could keep batteries within resistive heating limits and prolong battery life. One example is the ultrabattery, which combines a supercapacitor and a battery in one unit, creating an electric vehicle battery that lasts longer, costs less and is more powerful than current batteries used in plug-in hybrid electric vehicles.

1.4.2 Consumer electronics

As other capacitors, super-capacitors are extensively used as power back-ups for memory functions in a wide range of consumer products, such as cell phones and laptops. Furthermore, EDLCs can also be used in flashlights, portable media players, PC cards, flash photography devices for digital cameras, and in automated meter reading, particularly where extremely fast charging is desirable.

1.4.3 Alternative energy

The idea of replacing batteries with capacitors in conjunction with novel energy sources became a conceptual umbrella of the Green Electricity (GEL) Initiative, introduced by Dr. Alexander Bell.[12] One successful GEL Initiative concept was a muscle-driven autonomous solution that employs a multifarad EDLC as energy storage to power a variety of portable electrical and electronic devices such as MP3 players, AM/FM radios, flashlights, cell phones, and emergency kits. Moreover, EDLCs could be used for energy storage for solar panels as well.

1.5 Motivation

Studying the behavior of DC as a function of the electrode potential is essential in developing any EDL model, from the early Gouy-Chapman approximation[7-8] to the more recent Kornyshev formulation[13] or the Lamperski treatment.[14] Two DC shapes have been characterized by researchers: camel-shaped (or U-shaped),[15] defined by a minimum near the potential of zero charge

(PZC) flanked by two maxima at larger potentials; and bell shaped,[15-16] with one single maximum near PZC. Nevertheless, the reason why DC shows different dependence on electrode potential for different electrode/electrolyte systems is only partially understood.

Ohsaka et al. have reported that different shapes of DC curves could result from varied electrodes.[15] System temperature and electrolyte density, suggested by Lamperski et al., are also very important factors in determining the character of DC: high density and high temperature promote a bell-shaped DC.[14] Korneyshev suggested that exclusion steric effects and electrolyte compressibility within electric double layer plays a significant role in determining the shape of DC curve.[13] A U-shaped DC curve indicates either a weakly populated electrode surface or a large compressibility of electrolyte within the electric double layer. As the compressibility decreases, DC will increase at small potentials and then eventually decrease, forming a camel-shaped DC curve. When the exclusion effects are dominant and no further ions can be packed near the electrode surface, DC reaches the maximum near PZC and decreases with potential increases, which results in a bell-shaped DC.

Although the influence on DC of temperature, density,[14] polarizability[17] and compressibility[18] of RTILs are becoming understood, the role of electrode surface topography on DC remains unclear and maybe controversial. Lockett et al. found a bell-shaped DC curve for 1-butyl-1-methylpyrrolidinium/TFSI on both glassy carbon electrode and polycrystalline Au and Pt electrodes.[16] In contrast, Ohsaka et al. revealed a U-shaped DC curve for glassy carbon electrode and bell-shaped

DC curves on Au and Pt electrodes, both employing N,N-diethyl-N-methyl-N-(2-methoxyethyl) ammonium/TFSI electrolyte.[15]

Moreover, the variability of DC results for poorly prepared polycrystalline electrodes may indicate a strong dependence of DC on surface topography of electrode. Recently, Su et al. reported a strong dependence of structure of innermost electrolyte at the electrode/electrolyte interface on Au(001) surface topography, suggesting a significant impact of electrode surface structure on the innermost electrolyte structure and shape of DC curve.[19]

1.6 References

1. Conway, B. E., *Electrochemical supercapacitors : scientific fundamentals and technological applications*. Kluwer Academic / Plenum Publishers: New York, 1999; p 183.

2. Qu, D., Studies of the activated carbons used in double-layer supercapacitors. *Journal of Power Sources* **2002,** *109*, 403-411.

3. Liu, C.; Yu, Z.; Neff, D.; Zhamu, A.; Jang, B. Z., Graphene-based supercapacitor with an ultrahigh energy density. *Nano Letters* **2010**, 4863-4868.

4. An, K. H.; Kim, W. S.; Park, Y. S.; Moon, J.-M.; Bae, D. J.; Lim, S. C.; Lee, Y. S.; Lee, Y. H., Electrochemical properties of high-power supercapacitors using single-walled carbon nanotube electrodes. *Advanced Functional Materials* **2001,** *11*, 387-392.

5. Lerner, E. J., Less is more with aerogels: A laboratory curiosity develops practical uses. *The Industrial Physicist* **2004**, 26-30.

6. Yushin, G.; Dash, R.; Jagiello, J.; Fischer, J. E.; Gogotsi, Y., Carbide-derived carbons: Effect of pore size on hydrogen uptake and heat of adsorption. *Advanced Functional Materials* **2006,** *16*, 2288-2293.

7. McLaughlin, S., The electrostatic properties of membranes. *Annual Review of Biophysics and Biophysical Chemistry* **1989,** *18*, 113-36.

8. Chapman, D. L., A Contribution to the theory of electrocapillarity. *The London, Edinburgh, and Dublin Philosophical Magazine and Journal of Science* **1913,** *25*, 475-481.

9. Oldham, K. B., A Gouy–Chapman–Stern model of the double layer at a (metal)/(ionic liquid) interface. *Journal of Electroanalytical Chemistry* **2008,** *613*, 131-138.

10. Grahame, D. C., The electrical double layer and the theory of electrocapillarity. *Chemical Reviews* **1947,** *41*, 441-501.

11. Lyklema, J., *Fundamentals of interface and colloid science*. Academic Press: New York, 1995; Vol. 2.

12. Mathúna, C. O.; O'Donnell, T.; Martinez-Catala, R. V.; Rohan, J.; O'Flynn, B., Energy scavenging for long-term deployable wireless sensor networks. *Talanta* **2008,** *75*, 613-23.

13. Kornyshev, A. a., Double-layer in ionic liquids: paradigm change? *The Journal of Physical Chemistry. B* **2007,** *111*, 5545-57.

14. Lamperski, S.; Outhwaite, C. W.; Bhuiyan, L. B., The electric double-layer differential capacitance at and near zero surface charge for a restricted primitive model electrolyte. *The Journal of Physical Chemistry. B* **2009,** *113*, 8925-9.

15. Islam, M. M. A., M. T.; Ohsaka, T., Electrical double-layer structure in ionic liquids: A corroboration of the theoretical model by experimental results. *Journal of Physical Chemistry C* **2008,** *112*, 16568-16574.

16. Lockett, V.; Horne, M.; Sedev, R.; Rodopoulos, T.; Ralston, J., Differential capacitance of the double layer at the electrode/ionic liquids interface. *Physical Chemistry Chemical Physics : PCCP* **2010,** *12*, 12499-512.

17. (a) Lauw, Y.; Horne, M.; Rodopoulos, T.; Leermakers, F., Room-temperature ionic liquids: Excluded volume and ion polarizability effects in the electrical double-layer structure and capacitance. *Physical Review Letters* **2009,** *103*, 1-4; (b) Tazi, S.; Salanne, M.; Simon, C.; Turq, P.; Pounds, M.; Madden, P. a., Potential-induced ordering transition of the adsorbed layer at the ionic liquid/electrified metal interface. *The Journal of Physical Chemistry. B* **2010,** *114*, 8453-9.

18. Trulsson, M.; Algotsson, J.; Forsman, J.; Woodward, C. E., Differential capacitance of room temperature ionic liquids: The role of dispersion forces. *The Journal of Physical Chemistry Letters* **2010,** *1*, 1191-1195.

19. Su, Y.-Z.; Fu, Y.-C.; Wei, Y.-M.; Yan, J.-W.; Mao, B.-W., The electrode/ionic liquid interface: electric double layer and metal electrodeposition. *Chemphyschem : A European Journal of Chemical Physics and Physical Chemistry* **2010,** *11*, 2764-78.

CHAPTER 2

METHOD

Molecular dynamics simulations were performed to study the influence of electrode surface topography on the structure and differential capacitance of the electric double layer capacitor. MD simulations allow us to investigate single crystal or perfectly flat electrode surfaces, which are difficult or expensive to test experimentally. Besides, MD simulations provide insight at atomic level on the mechanism of the investigated charge and discharge processes. Furthermore, MD simulations single out and investigate each factor that is inherently difficult to separate in experiments. In this work, the polarizability of APPLE&P force field was turned off to describe the interactions among atoms. Any sorts of terminated atoms were also eliminated from the flat and the rough graphite surfaces. All these actions were taken to study the pure effect of electrode surface topography on the electric double layer structure and differential capacitance.

The simulation setups, consisted of a molten ionic liquid electrolyte inserted between two graphite electrodes, were shown in Figures 2.1(a) and 2.1 (b). Snapshots showing the specific surface topography of electrodes were given in Figures 2.2(a) and 2.2(b). The successive hexagonal graphite layers were stacked in ABAB sequence. We found that the crystallographic orientation of the

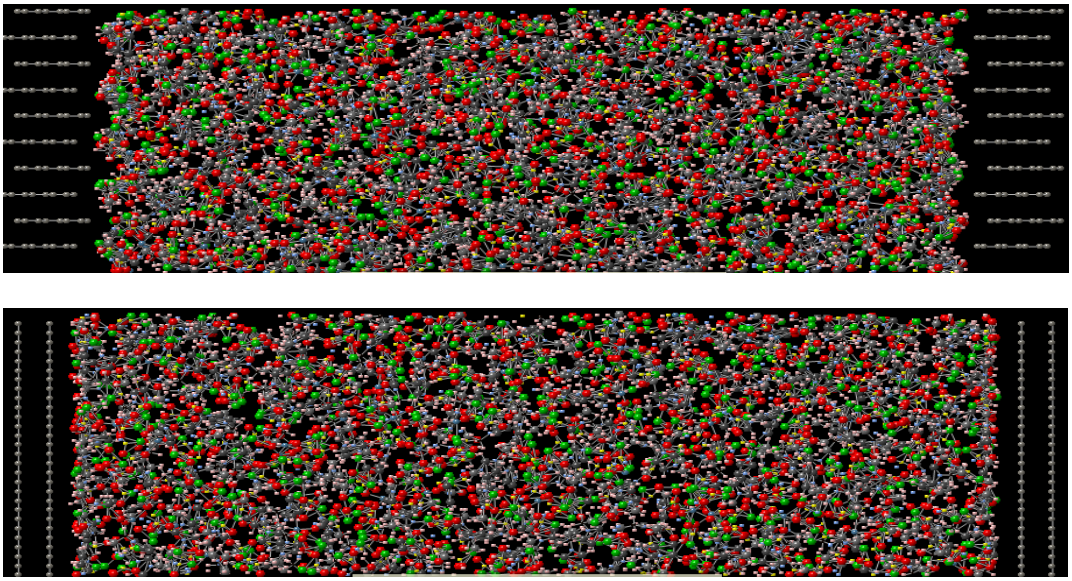

(a)

(b)

Figure 2. 1 Snapshots realing the system setup. (a) molecularly rough surface EDLC and (b) molecularly flat surface EDLC.

graphite carbon atoms changed the electrode surface roughness and formed two different electrodes: one was graphite with edge orientation and the other was graphite with flat basal plane. Throughout this thesis, the surface with flat basal plane would be referred as flat surface and the surface with edge orientation as rough surface. Additionally, the ionic liquid electrolyte contained 240 1-ethyl-3-methyl imidazolium ($EMIM^+$), 310 bis-fluorosulfonyl imide (FSI^-), and 70 Li^+. In other words, 240 EMIMFSI solvent molecules and 70 LiFSI salt molecules were employed as an electrolyte in our two EDLCs. The molecular structures of $EMIM^+$ and FSI^- with atom notations were given in Figures 2.3(a) and 2.3(b). This particular ionic liquid electrolyte was chosen largely due to its nonflammability, low vapor pressure and large electrochemical window.

Ahead of this project, properties of the bulk ionic liquid electrolyte (EMIMFSI with LiFSI) had already been reported. Nevertheless, the bulk electrolyte was simulated in a cubic box, so the cubic box was changed into an orthorhombic box first. The X and Y axes values were set according to the dimension of electrodes, and Z axis was calculated to make sure the orthorhombic box had same volume as the cubical one, such that ions' number density in the two boxes were the same. Then, the bulk electrolyte system was run until the molecules randomly distributed in the box and the pressure tensor in XY plane (parallel to electrode surface) and Z direction (normal to electrode surface) reached zero. Next, graphite electrodes with different crystallographic orientation were added into the two systems. Then, systems were run again to adjust the box size until the pressure tensors reached zero. Later, we applied

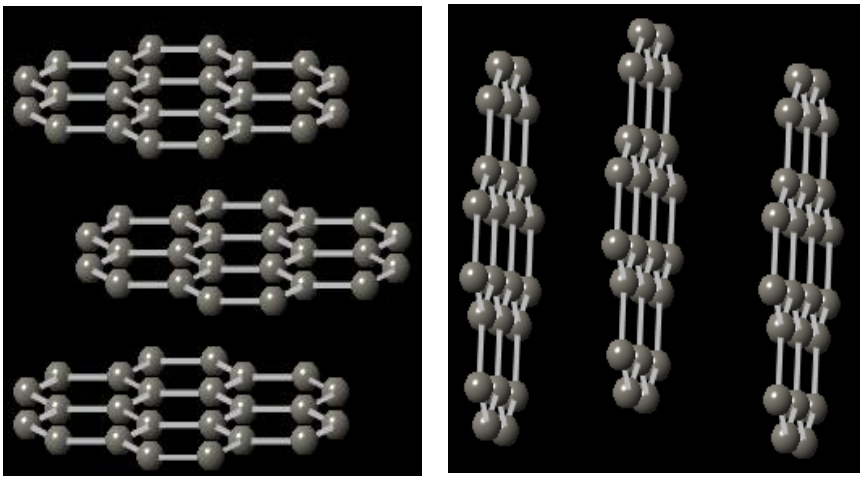

(a) (b)

Figure 2. 2 Crystallographic orientations of graphite electrodes. Panel (a) and (b) are snapshots of crystallographic orientations of graphite with edge orientation and graphite with flat basal plane respectively.

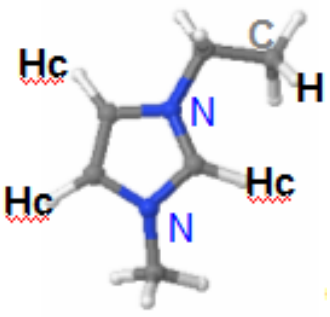

(a)

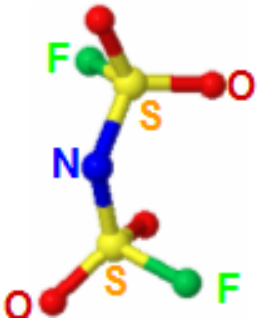

(b)

Figure 2. 3 Molecular structure of electrolyte. The panel (a) and (b) show the molecular structure of $EMIM^+$ and FSI^- as well as the atom notation utilized in this work.

twenty different potentials between electrodes at 393 K and eight different potentials at 453 K in both the flat electrode surface and the rough electrode surface EDLCs, as shown in Table 2.1. Subsequently, we calculated the electric double layer potential by subtracting the potential of zero charge from the potential drop between electrode and electrolyte. Afterwards, the EDLC systems with potentials were run again for 2.5 nanoseconds for equilibration. Finally, the production run began for a total time of 50 ns and data were collected for further analysis.

The potential difference between electrodes was controlled by minimizing the total electrostatic energy of the system with respect to the electrode charges, as described in Refs[1]. This scheme to assign the electrode charges was expected to correctly reproduce the charge distribution on the highly conductive surfaces. It was particularly important to obtain the correct charge distribution on the rough surface because not all rough surface atoms were equivalent. These simulations were run in the NVT ensemble. Furthermore, the temperature was controlled with a Nose Hoover thermostat,[2] having a coupling constant of 0.1 picosecond. The interactions between atoms were modeled using the APPLE&P[3] force field with polarization turned off. The influence of polarization on the bulk [EMIM][FSI] structure, transport and thermodynamics were reported previously.[4] Additionally, the short-range interactions (dispersion and real space Ewald) were evaluated within a spherical cut-off of 10 Å and the Fourier part of Ewald was evaluated with computationally expedient SPME adapted for 2D geometry.[5]

Systems' configuration, density, charge, potential energy and total energy

Table 2.1

Potential Difference Across EDLCs

	Potential									
393 K	6.80	6.40	6.00	5.60	5.00	4.50	4.00	3.50	3.00	2.70
	2.50	2.20	2.00	1.60	1.30	1.00	0.80	0.50	0.25	0.00
453 K	6.80	5.60	4.00	3.00	2.00	1.00	0.50	0.00		

data were collected every five picosecond. Molecular number density profiles were plotted as a function of their center of mass to show the structures of EDLs. The potential of zero charge (PZC) was calculated from the potential drop within electrical double layer (EDL) at the potential difference between electrodes of 0 V. At 393 K, the PZCs were -0.19 V and -0.27 V for the flat and rough surface respectively; at 453 K, the corresponding PZCs were -0.20 V and -0.27 V. In this work, we defined the electrode potential as the potential drop within EDL relative to the PZC:

$$U_{RPZC}=U_{EDL}\text{-}PZC=U_{elctrode}\text{-}U_{bulk}\text{-}PZC \quad (2.1)$$

Specifically, the EDL potentials were calculated by integrating the plane-averaged (xy plane) 1-D Poisson equation for the charge density profiles along the direction normal to electrode surface (z axis). Capacitance is calculated using the following equation:

$$C = \frac{Q}{V} \quad (2.2)$$

Then, the differential capacitances were obtained by fitting a parabola over the local behavior of the electrode charge versus potential using the method described in Ref., [6] and further confirmed by fitting higher order (fourth and fifth) polynominals over the extended potential range.

This chapter has explained systems' setup, simulation procedure and control parameters, and result analysis methods used in this qualitative study of effect of electrode surface topography on the electric double layer's structure and differential capacitance. The next chapter will present the results obtained with

this molecular dynamics simulations method and how we interpreted the date.

2.1 References

1. (a) Reed, S. K.; Lanning, O. J.; Madden, P. a., Electrochemical interface between an ionic liquid and a model metallic electrode. *The Journal of Chemical Physics* **2007,** *126*, 084704; (b) Vatamanu, J.; Borodin, O.; Smith, G. D., Molecular dynamics simulations of atomically flat and nanoporous electrodes with a molten salt electrolyte. *Physical Chemistry Chemical Physics : PCCP* **2010,** *12*, 170-82.

2. Tanibayashi, S.; Tada, T.; Watanabe, S.; Yoshizawa, K., Computational study on stable structures, formation energies, and conductance of single benzene-dithiolate between two Au electrodes. *Japanese Journal of Applied Physics* **2005,** *44*, 7729-7731.

3. (a) Borodin, O.; Smith, G. D., Structure and dynamics of N-methyl-N-propylpyrrolidinium bis(trifluoromethanesulfonyl)imide ionic liquid from molecular dynamics simulations. *The Journal of Physical Chemistry. B* **2006,** *110*, 11481-90; (b) Borodin, O., Polarizable force field development and molecular dynamics simulations of ionic liquids. *The Journal of Physical Chemistry. B* **2009,** *113*, 11463-78; (c) Smith, G. D.; Borodin, O.; Russo, S. P.; Rees, R. J.; Hollenkamp, A. F., A molecular dynamics simulation study of LiFePO4/electrolyte interfaces: structure and Li+ transport in carbonate and ionic liquid electrolytes. *Physical Chemistry Chemical Physics : PCCP* **2009,** *11*, 9884-97; (d) Borodin, O.; Gorecki, W.; Smith, G. D.; Armand, M., Molecular dynamics simulation and pulsed-field gradient NMR studies of bis(fluorosulfonyl)imide (FSI) and bis[(trifluoromethyl)sulfonyl]imide (TFSI)-based ionic liquids. *The Journal of Physical Chemistry. B* **2010,** *114*, 6786-98.

4. Bedrov, D.; Borodin, O.; Li, Z.; Smith, G. D., Influence of polarization on structural, thermodynamic, and dynamic properties of ionic liquids obtained from molecular dynamics simulations. *The Journal of Physical Chemistry. B* **2010,** *114*, 4984-97.

5. (a) Kawata, M.; Mikami, M., Rapid calculation of two-dimensional Ewald summation. *Chemical Physics Letters* **2001,** *340*; (b) Kawata, M.; Mikami, M.; Nagashima, U., Rapid calculation of the Coulomb component of the stress tensor for three-dimensional systems with two-dimensional periodicity. *The Journal of Chemical Physics* **2001,** *115*, 4457; (c) Kawata, M.; Nagashima, U., Particle mesh Ewald method for three-dimensional systems with two-dimensional periodicity. *Chemical Physics Letters* **2001,** *340*, 165-172; (d) Kawata, M.; Mikami, M.; Nagashima, U., Response to “Comment on ‘Rapid calculation of the Coulomb component of the stress tensor for three-dimensional systems with two-dimensional periodicity’□” [J. Chem. Phys. 117, 3524 (2002)]. In *The Journal of Chemical Physics*, 2002; Vol. 117, p 3526; (e) Kawata, M.; Mikami, M.;

Nagashima, U., Computationally efficient method to calculate the Coulomb interactions in three-dimensional systems with two-dimensional periodicity. *The Journal of Chemical Physics* **2002,** *116*, 3430.

6. Fedorov, M. V.; Kornyshev, A. a., Ionic liquid near a charged wall: structure and capacitance of electrical double layer. *The Journal of Physical Chemistry. B* **2008,** *112*, 11868-72.

CHAPTER 3

RESULTS AND DISCUSSION

In this work, we use molecular dynamics simulations to show that the electrode surface topography of EDLC could qualitatively change the shape of the differential capacitance (DC) curve, especially near PZC. Specifically, the flat surface EDLC generates a camel-shaped DC curve, while the rough surface EDLC engenders a bell-shaped DC curve. Section 3.1 compares the crystallographic structure of graphite electrodes with the flat basal plane and that with edge orientation, and details surface roughness between the flat and the rough electrode. Zero positions of electrodes are defined in this section as well. In section 3.2, the camel-shaped and bell-shaped DC curves are compared and explained from the point of view of the electrode charge. Then, potential energy of $EMIM^+$ and FSI^- as a function of distance from electrode surface is given in section 3.3, to elucidate ions' distributions on electrode surfaces detailed in section 3.4. Section 3.5 presents molecular number densities in terms of electrode potential to illustrate the reason why two different shapes of DC curve are formed. Lastly, section 3.6 offers the coordination number of O (FSI^-) ($EMIM^+$) and O (FSI^-)–N ($EMIM^+$) to further explain how electrolyte structure in electrode/electrolyte interface affects the DC curve of an EDLC.

3.1 Topography and zero position of electrode surface

The simulation setup consists of a room temperature ionic liquid (RTIL) inserted between two graphite electrodes. The successive hexagonal graphite layers are stacked in ABAB sequence. Snapshots showing the specific crystallographic structure of graphite electrodes in contact with the electrolyte are given in Figure 3.1. The distance between consecutive graphite sheets is 3.35 Å. We have also measured the distance between innermost and outermost carbon atoms next to the electrolyte to illustrate the electrode surface roughness. This distance is 0 Å for the flat basal-plane graphite and 1.42 Å for the rough-edge graphite, along the direction normal to the electrode surface.

In order to describe electrode/electrolyte interface more easily, it is necessary to define zero positions of electrodes. As shown in Figure 3.2, the zero position of the flat surface is the center of mass of the graphite sheet exposed to the electrolyte. For the rough surface electrode, the zero position of the electrode is defined according to the flat surface such that maxima of the ions' density profiles of the two EDLCs are largely overlapped. Utilizing the above definition of the zero positions of electrodes, we verified both the first and second peaks of the ions' density profiles located at roughly similar distance from the electrode for both electrodes. Moreover, to better understand the EDL structure, we divided the EDL into two layers based on the density profiles of electrolyte ions: the first layer, located between 2.2 Å and 5.3 Å from the electrode; and the second layer, located between 5.3 Å to 7.5 Å from the electrode. 2.2 Å was chosen because no ion penetrates closer than 2.2 Å from the electrodes.

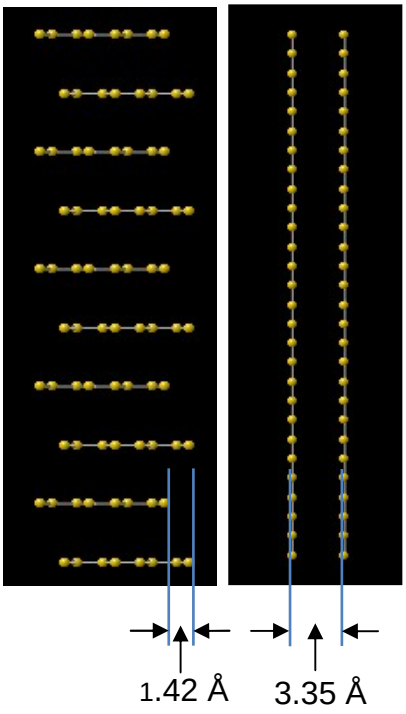

Figure 3. 1 Cropped image snapshots showing lateral view of graphite electrodes. (a) graphite with edge orientation, (b) graphite with flat basal plane. The graphene layers are stacked such that edge atoms of consecutive layers are shifted along our asymmetry direction (z-axis) by 1.42 Å, generating a molecularly rough surface.

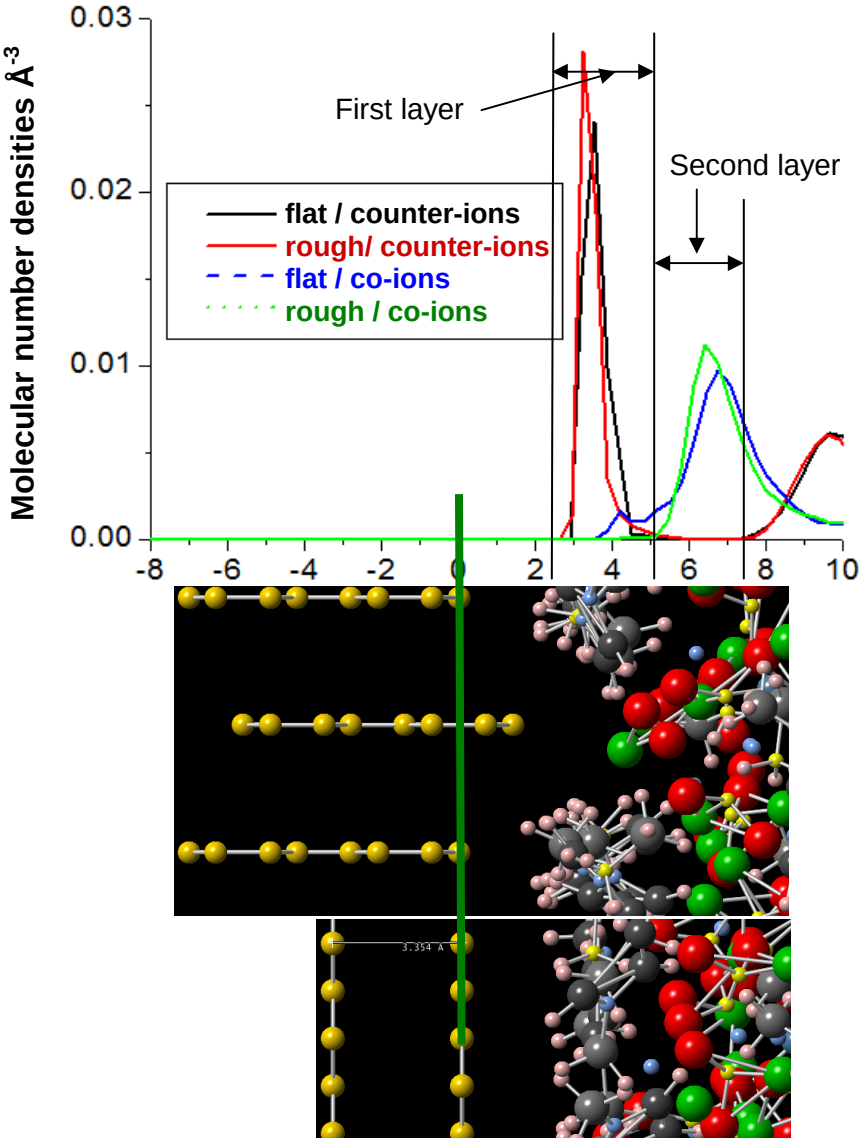

Figure 3. 2 Division in layers of SEI and zero positions of electrodes. The particular systems presented here are negative electrodes charged at -2.7 V_{RPZC}. The first image above (a) shows the density profiles of $EMIM^+$ (red and black line for rough and flat surface) and of FSI^- (green and blue for rough and flat surface). The black vertical lines in plot (a) indicate our division of layers of the electrolyte. The first cropped image snapshot (b) shows the zero position of the rough electrode. The second cropped image snapshot (c) shows the zero position of the flat electrode.

3.2 Camel-shaped and bell-shaped DC curves

The DC curves are qualitatively different for the two super-capacitors with different electrodes. The dependence of DC on electrode potential for the flat and rough surface super-capacitors is shown at 393 K in Figure 3.3a. Specifically, the flat surface EDLC generates a camel-shaped DC curve with a local minimum at around -0.8 V_{RPZC} and two maximum at -1.5 V_{RPZC} and +0.6 V_{RPZC}. Alternately, the rough surface EDLC generates an overall bell-shaped DC curve with a maximum at -0.3 V_{RPZC}. The DC value near PZC is significantly larger (almost double) for the rough surface EDLC compared to the flat one. For example, at the potential of -0.3 V_{RPZC}, the DC is 9.6 μF/cm2 for the rough surface system and 5.6 μF/cm2 for the flat surface system. Moreover, at a potential more negative than -1.26 V_{RPZC}, the DC of the rough surface system is smaller than that of the flat surface system. In other ranges of electrode potential, the rough surface system always shows a larger DC value than the flat surface system.

Figure 3.3b displays the corresponding electrode charge in terms of applied electrode potential at 393 K. This figure shows that the electrode charge changes faster in the rough surface system than it does in the flat surface system at relatively low electrode potentials. The fast change of the electrode charge is consistent with the large differential capacitance in the rough surface system. It can also be found in Figure 3.3b that in the flat surface system, the shape of the electrode charge curve is close to a linear line; in contrast, in the rough surface system, the slope is deeper in low electrode potentials than in large potentials. This phenomenon is consistent with the fact that the DC of the flat surface has a

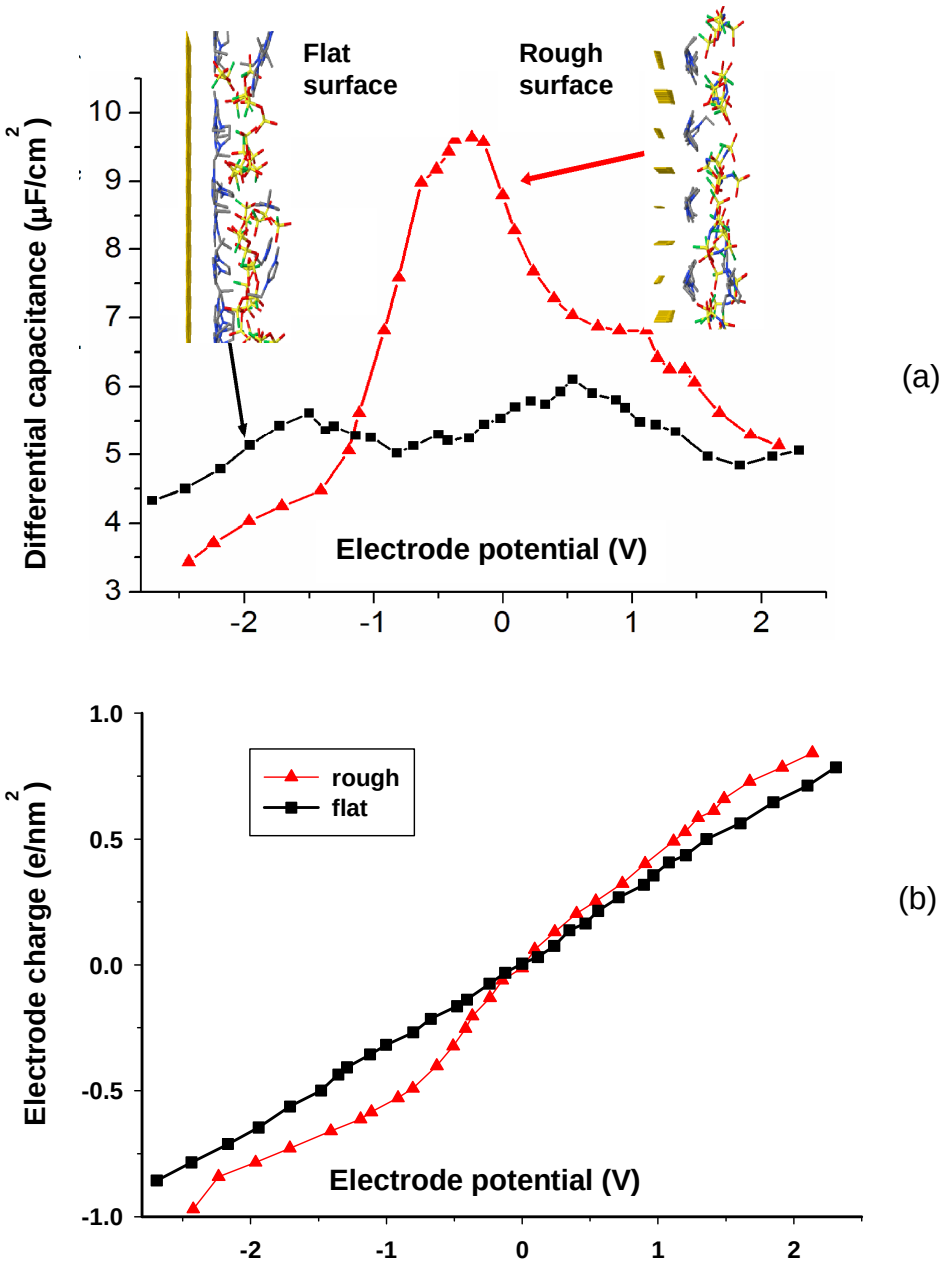

Figure 3. 3 Differential capacitance and electrode charge as a function of electrode potential at 393 K. (a) Dependence of differential capacitance on electrode potential for the flat and the rough electrode surface EDLCs. Inset are image snapshots indicating the electrolyte structuring pattern on the flat (left inset) and the rough (right inset) surfaces at about -2.5 V_{RPZC}. (b) Dependence of electrode charges in terms of electrode potential for the flat (black line) and the rough (red line) electrodes at 393K.

smaller oscillation than the rough one. The observation of the camel-shaped DC curve for the flat surface EDLC is not surprising since this shape has previously been observed in similar systems with pyr13/TFSI and pyr13/FSI between two flat surface electrodes.[1, 2] In our previous work, the camel-shaped DC curve resulted from ions' rearrangement within EDL upon changing the electrode potential.[3] The bell-shaped DC curve has also been observed before in other super-capacitors.[4, 5] However, it is striking that the shape of DC curve changes qualitatively, from a camel-shape to a bell-shape if the basal-plane graphite is replaced with the edge orientation graphite. It should be addressed that the degree of surface roughness is very small: 1.42 Å.

As shown in Figures 3.4a and 3.4b, the results of simulations at 453 K exhibit similar qualitative trends of DC curves as a function of electrode potential, which further confirms the reproducibility of our results.

3.3 Potential energy of $EMIM^+$ and FSI^-

To understand why $EMIM^+$ and FSI^- separate into different layers at the rough surface and mix together at the flat surface, we calculated their nonbonded potential energy as a function of ions' center of mass relative to electrodes. Specifically, nonbonded potential energy of $EMIM^+$ and FSI^- are computed at PZC, where the difference in DC values between the two systems is large (see Figure 3.3a).

According to Figure 3.5, the nonbonded potential energy of FSI^- within 6 Å from the flat electrode is smaller than that of the bulk FSI^- by 20-30 KJ/mol. Moreover, there are several local minima of FSI^- potential energy in the first and

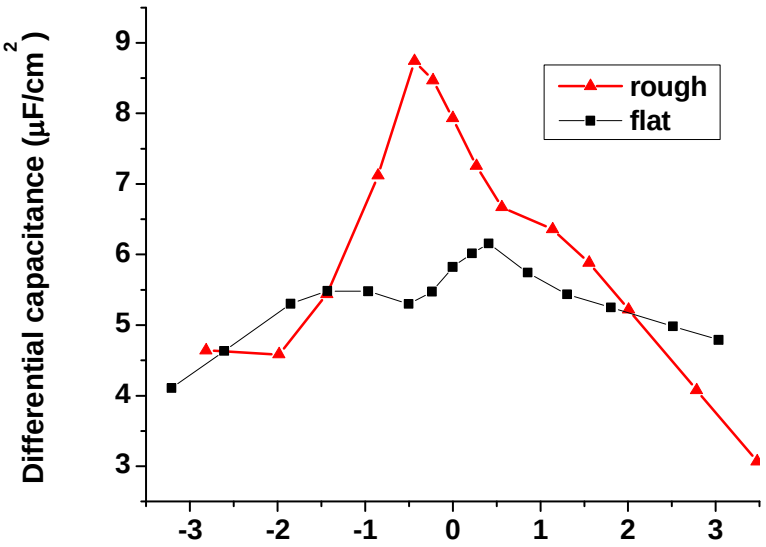

(a)

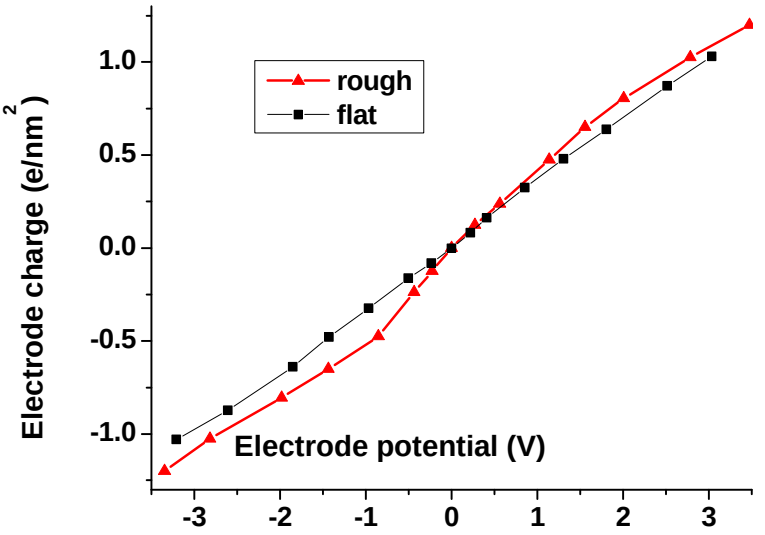

(b)

Figure 3. 4 Differential capacitance and electrode charge as a function of electrode potential at 453 K. (a) Differential capacitance of the EDLC with flat surface electrode (square) and rough surface electrode (triangle) at 453 K. (b) The corresponding electrode charge for the DC curves shown in (a).

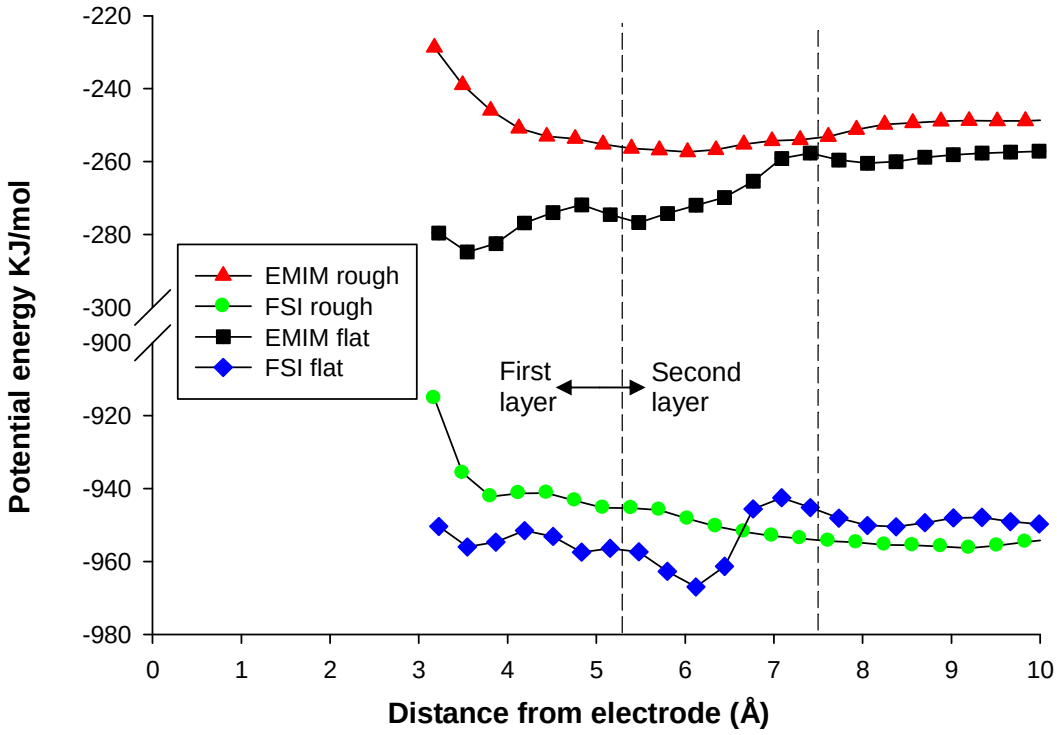

Figure 3. 5 The nonbonded potential energy. The nonbonded potential energy of $EMIM^{+}$ and FSI^{-} as a function of distance from the electrode for the rough and the flat surface EDLC.

the second layer, so FSI^- ions are trapped in the local minimum positions in the interface. In contrast, for the rough surface, the non-bonded potential energy of FSI^- within ~3.5 Å is higher than that beyond 3.5 Å by about 30 KJ/mol so that FSI^- ions at the rough surface prefer to move away from the first layer. Furthermore, beyond 3.5 Å, the nonbonded potential energy is almost constant, hence FSI^- ions can easily shift between the first and second layer at the rough surface.

It is important to study whether the difference in ions' potential energy between two types of surfaces arise from the interaction between ions and electrode surfaces or from the interaction among electrolyte ions. Note that, at PZC, the electrostatic interaction between ions and electrode surfaces is defined as zero. In this regard, the nonbonded potential energy is decomposed into contributions from electrostatic interaction and van der Waals interaction. Take FSI^- for example, the van der Waals interaction (between FSI and its environment) has contributed less than 4 KJ/mol for the potential energy difference (about 20 KJ/mol). This means that the difference in potential energy is due primarily to the difference in electrostatic interaction of electrolyte ions, rather than the ion-ion and the surface-electrolyte van der Waals interactions. Since the $EMIM^+$ and FSI^- separate into two layers at the rough surface and mix together at the flat surface, the electrostatic interactions between ions must be different at the two surfaces. As a result, the difference of electrode surface roughness changes electrolyte structuring at the electrode/electrolyte interface, which leads to the difference of electrostatic interactions between ions, and hence the difference of DC for the

two different surfaces. In the next section, molecular distributions at the flat and the rough surface will be given to show that ions' adsorption is strongly dependent on the electrode surface roughness.

3.4 $EMIM^+$ and FSI^- distributions on electrode surface

In order to clarify the difference in electrolyte structuring on the two surfaces, we plotted the distributions of $EMIM^+$ and FSI^- in our xy-plane (a planeparallel to the electrode surface). As shown in Figure 3.6, upper panels are image snapshots of the first layer electrolyte structure and bottom panels are density distributions of $EMIM^+$. These ions' density distributions are computed by binning ions' position of center of mass on a 20*20 grid on the plane. This procedure will not capture the detailed structure of ions near electrode surface, but rather the position of ions relative to the surface. In the bottom panels of Figure 3.6, at the flat surface, a random distribution of $EMIM^+$ in the first layer is found at PZC, because ions have no preference for certain surface sites; while, at the rough surface, structured distribution is observed at PZC since the first layer $EMIM^+$ are constrained to surface sites with microfacets. The distributions of the adsorbed ions in xy-plane are clearly different for the two types of surfaces. These density distribution profiles reveal that ion absorption depends heavily on the electrode surface topography.

While the ions are distributed randomly at the atomically flat surface, the ions near the rough surface are aligned parallel to the surface strips/microfacets, due to ions' tendency to preferentially sit on certain positions on the rough surface. According to Figure 3.7(1a), EMIMs in the first layer prefer to lie along

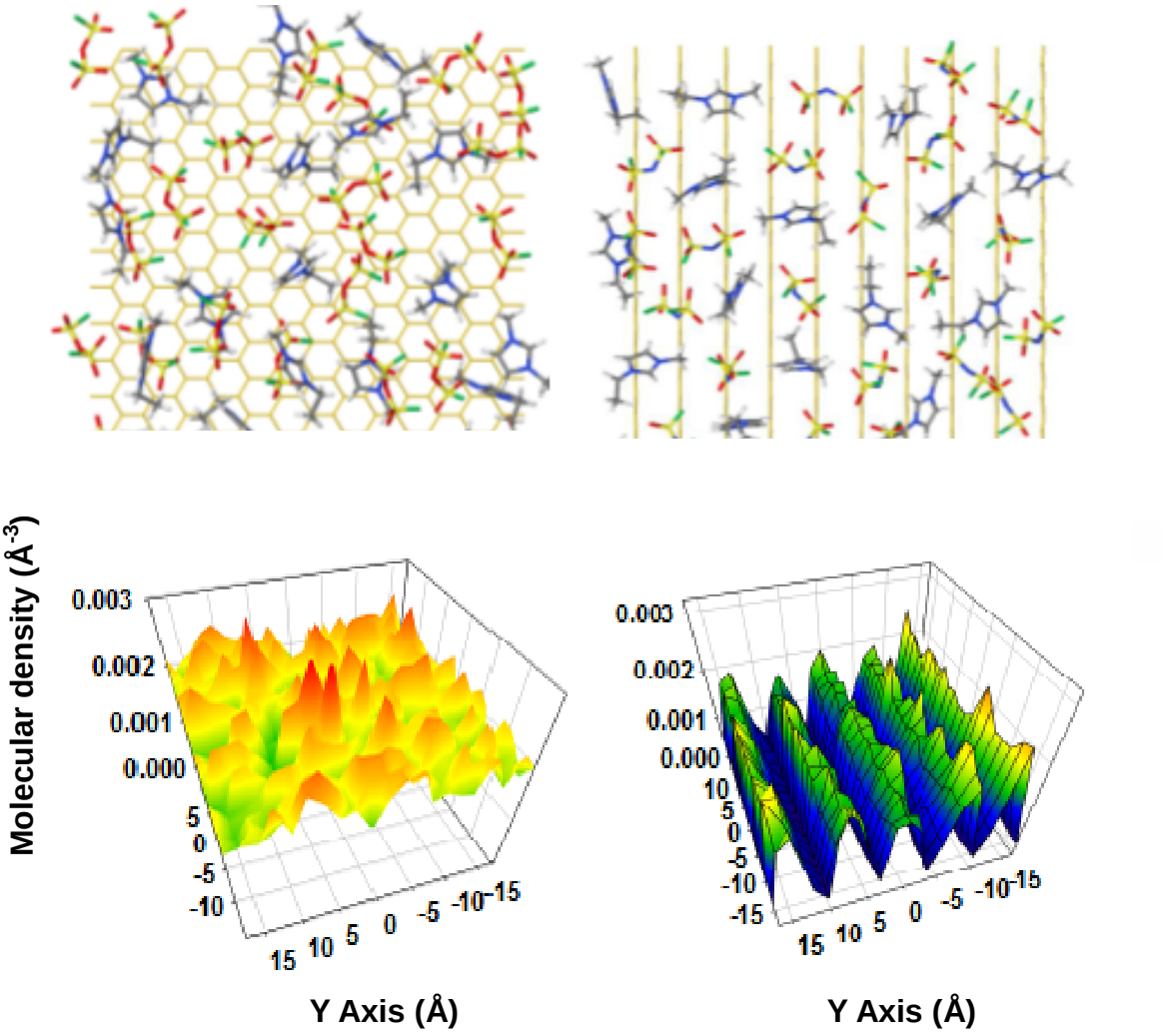

Figure 3. 6 Ions' distributions in xy-plane. A comparison of ions' distributions in xy-plane on the flat and the rough electrode surfaces. The upper panels are image snapshots of $EMIM^+$ and FSI^- in the first layer and the bottom panels are density profiles of $EMIM^+$ in the first layer. The blue/green areas represent low densities while the yellow/orange areas represent high densities of $EMIM^+$.

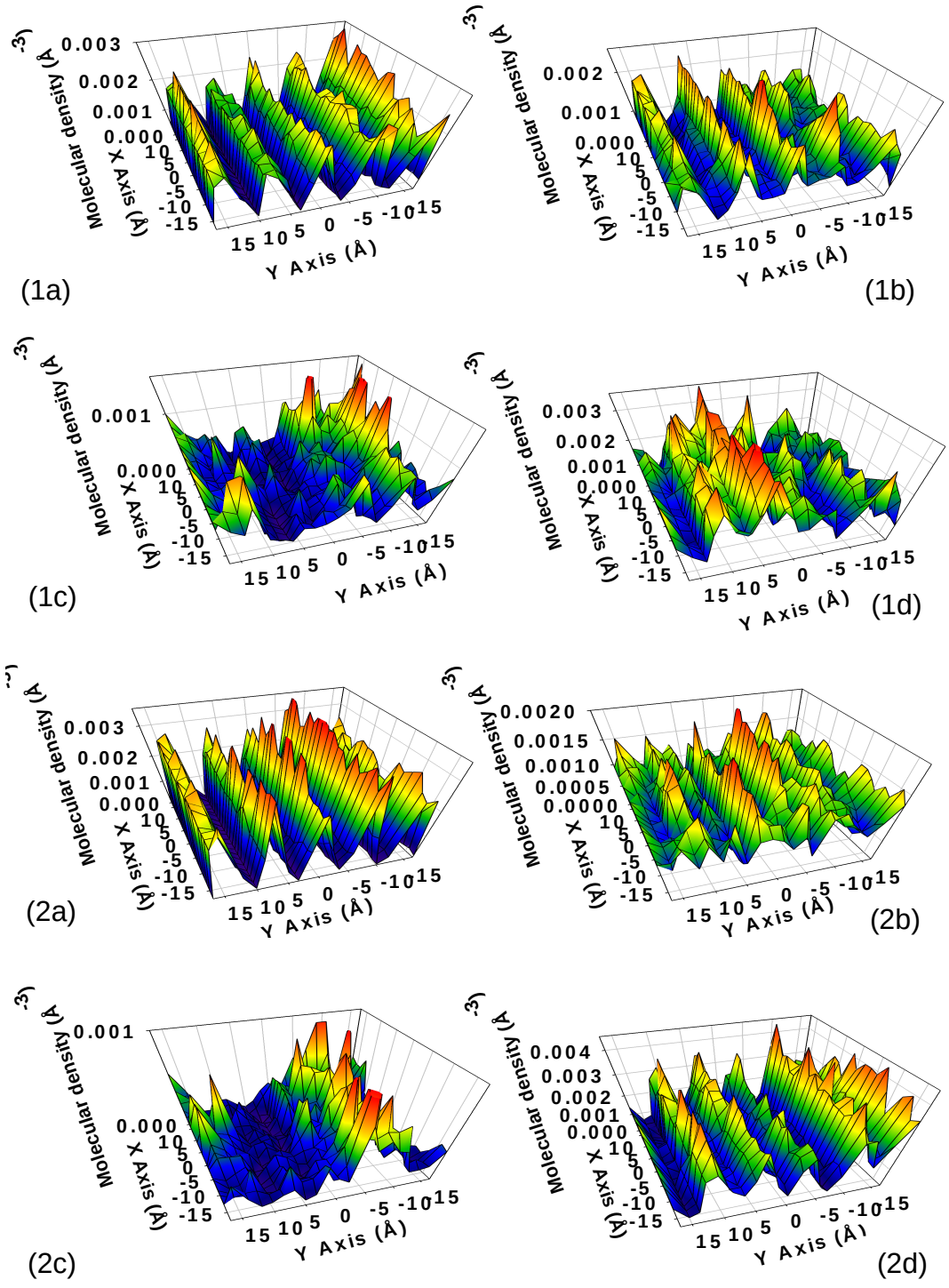

Figure 3. 7 Electrolyte distribution. Image snapshot showing the electrolyte distribution near the rough surface for first layer (panels 1a,1b,2a,2b) and second layer (panels 1c,1d,2c,2d) for $EMIM^+$ (panels 1a,1c,2a,2c) and FSI^- (panels 1b,1d,2b,2d) at -0.24 V_{RPZC} (panels 1) and -0.42 V_{RPZC} (panels 2).

the strips (microfacets) at the rough surface at -0.24 V_{RPZC}, while FSIs in the second layer are not structured yet at this particular potential. When we increase the potential at the electrodes to -0.42 V_{RPZC} (see Figure 3.7(2a)), the first layer EMIMs become more rigidly ordered, and even the FSIs in the second layer structure themselves in a similar pattern as the first layer EMIMs. By comparing panels 1 with panels 2, the density of first layer EMIM+ increases and the density of the second layer EMIM+ decreases on the rough surface. Similarly, the density of the second layer FSI- increase with the first layer FSI- decreases. This suggests that some of the second layer EMIMs move into the first layer and part of the second layer FSIs migrate into the second layer when increasing electrode potential.

Also shown in Figure 3.7, ions' distributions at different potentials at the rough surface are used to illustrate the ordering rates of EMIMs and FSIs. At low potentials (PZC to -0.4 V_{RPZC}), only the first layer electrolyte is structured in such a "corrugated" pattern, matching to the roughness of the surface. In the potential range -0.4 V_{RPZC} to -0.9 V_{RPZC} (where DC changes quickly with potential), we observed ordering in the second layer. At -0.24 V_{RPZC} the second layer shows little or no lateral structuring reflecting the underlying electrode structure, while at -0.42 V_{RPZC} the second layer is populated primarily by co-ions and is structured in a similar "corrugated" pattern as the first layer.

Note that the difference on structuring reported here is consistent with results of Su et al. for gold electrodes.[6] This affirms that the ordering of the absorbed electrolyte ions depends heavily on the surface topography.

3.5 Molecular densities in terms of electrode potential

Figure 3.8 shows the average number density of $EMIM^+$ and FSI^- in the first and second layers as a function of electrode potential in the two different systems. In the potential window, -1.0 V_{RPZC}~+0.5 V_{RPZC}, similar slopes of number density were observed for $EMIM^+$ in two different surfaces in both layers. This particular phenomena means that the changes of $EMIM^+$ density in the two layers are very similar for both surfaces. However, in the same potential window, the changes of FSI^- density with potential are more pronounced in both layers for the rough surface system. Therefore, it is likely that fast displacement of FSI^- from the rough surface with increasing negative potential is an important factor determining the larger magnitude of DC value and the overall bell-shaped DC curve.

Other features of DC curve are also in agreement with the average number density of ions as a function of EDL potential, as shown in Figure 3.8. The average number densities of the first layer $EMIM^+$, and the second layer FSI^- at the rough surface, remain essentially constant for a potential more negative than -1.26 V_{RPZC}, suggesting a fast saturation of ions' adsorption at the rough surface. This phenomenon is consistent with the observation that the DC of the rough surface is smaller than that of the flat surface beyond -1.26 V_{RPZC}. The fast saturation is also in agreement with the fact that, at a relatively low potential, the rough surface system shows a larger (almost double) DC value when compared to a flat surface system.

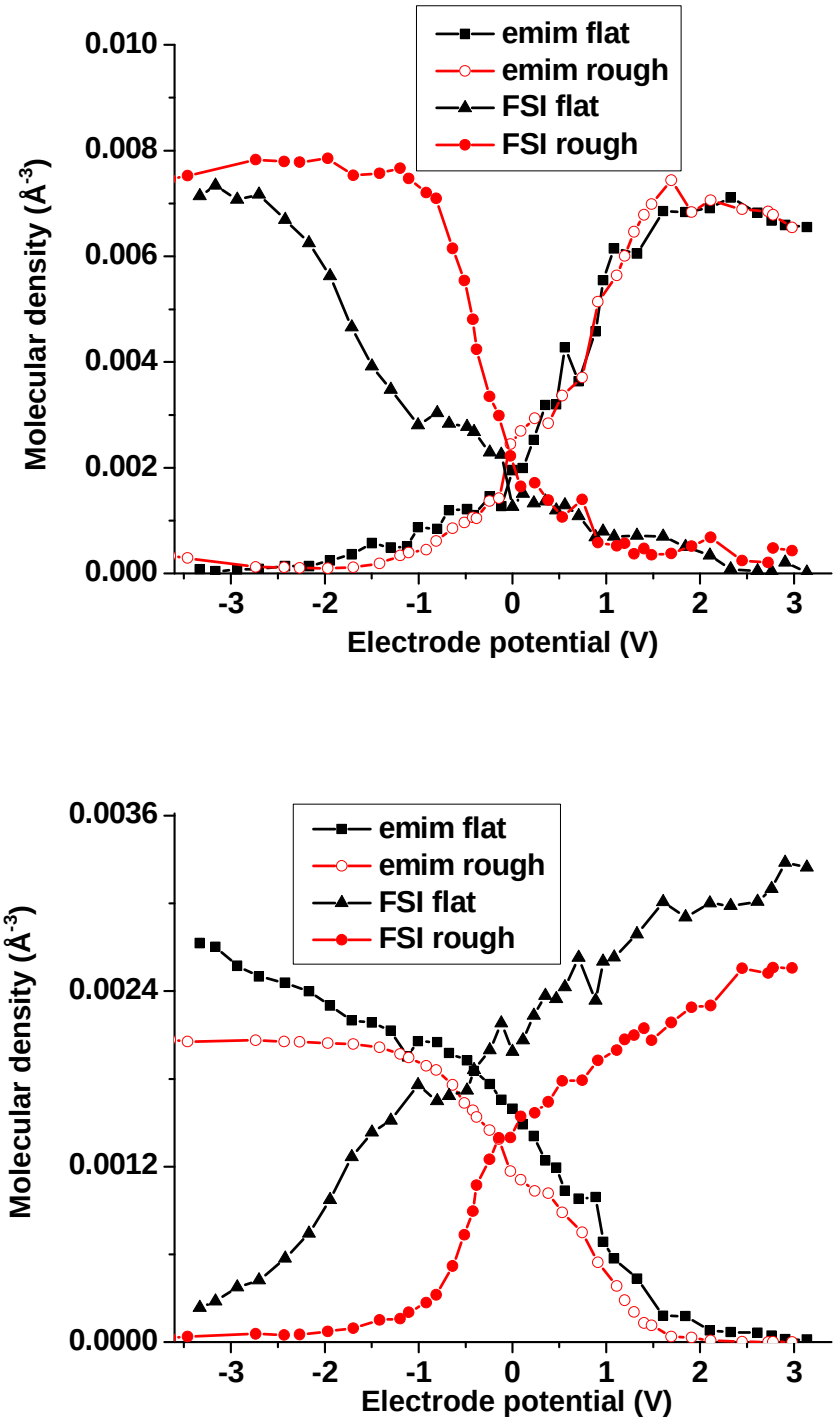

Figure 3. 8 The average number densities of EMIM+ and FSI- as a function of electrode potential. (a) the first layer and (b) the second layer.

3.6 Coordination number between O (FSI^-) and H ($EMIM^+$)

Shown in the Figure 3.9 is the coordination number between the O (FSI^-) in the innermost layer and H ($EMIM^+$) in various layers at PZC. The total coordination numbers between O and H from both layers are the same for both surfaces, indicating similar overall $EMIM^+$ densities as expected. However, the coordination number between the O and the first layer H is smaller for the rough surface system by about 20-25%, while the coordination number between O and the second layer H is larger for the rough surface system by about 20-25%, when compared to that of the flat surface system. Similar trends are observed for O (FSI)–N (EMIM), as shown in Figure 3.10.

These phenomena indicate that ions in the two layers at the rough surface are restructured such that there are fewer anion-cation bonds within the layer. Specifically, this means that cations and anions in electrode/electrolyte interface separated into the first and the second layer respectively at the rough surface, so there are more cation-anion bonds between the first and second layer. However, at the flat surface, cations and anions are mixed together in the two layers, such that more cation-anion bonds could be found within the same layer. Such re-arrangement near the rough surface might be expected to favor the displacement of ions between the first and the second layer upon changes in the electrode potential, generating a larger DC value near the rough surface.

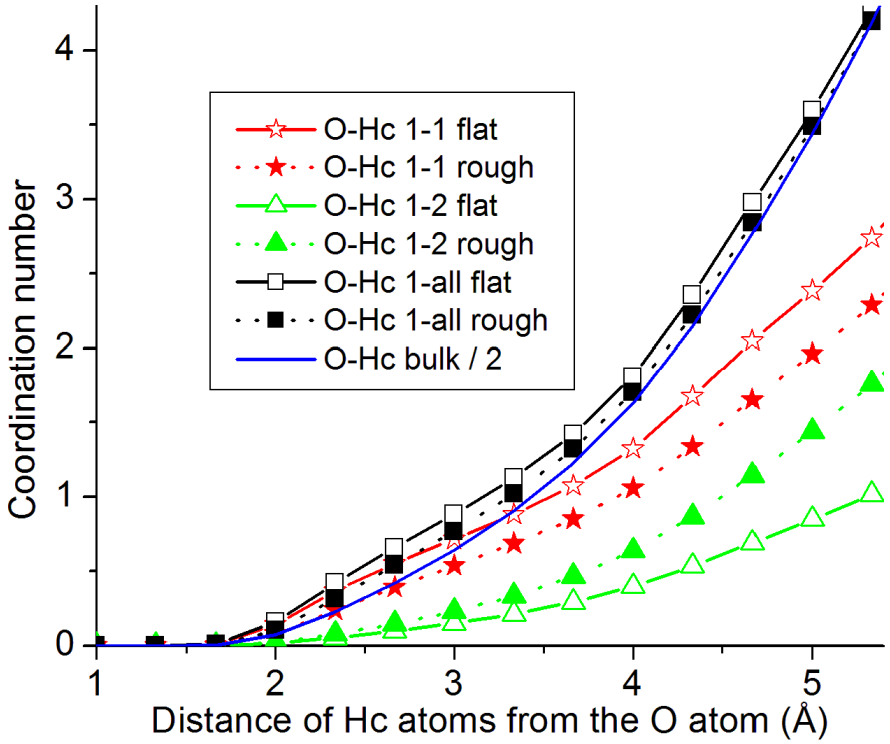

Figure 3. 9 Coordination number between O and H. The coordination number between the O (FSI^-) in the first layer and Hc ($EMIM^+$) in different layers. These coordination numbers were calculated accounting for i) Hc atoms from the first layer only, ii) Hc atoms from the second layer only, and iii) all Hc atoms regardless of their particular layer. The blue line represents half of the O-Hc coordination number calculated in bulk electrolyte.

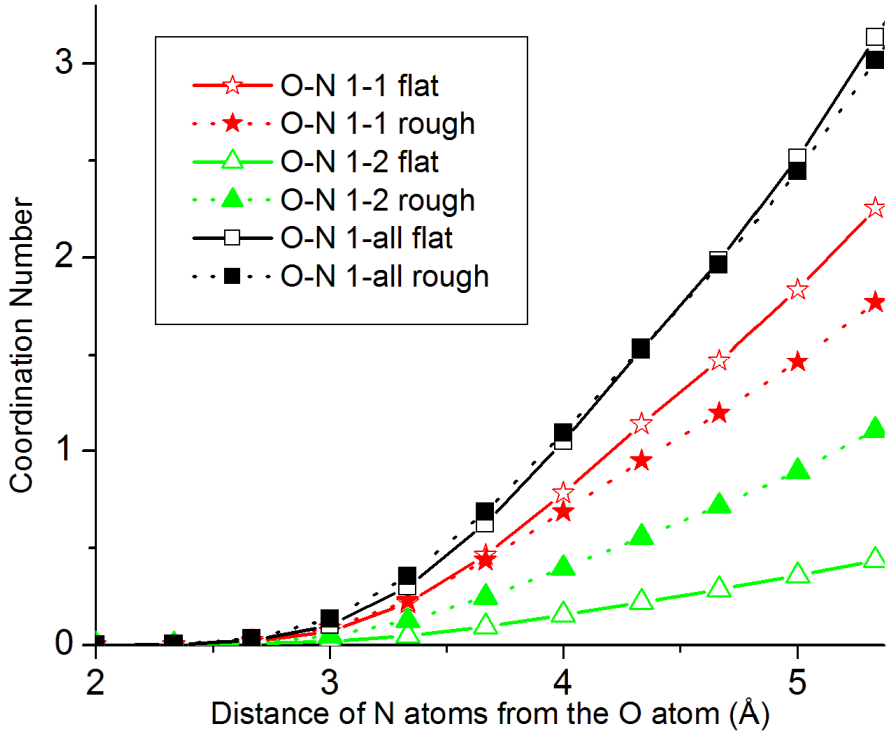

Figure 3. 10 Coordination number between O and N. The coordination number between the O (FSI^-) in the first layer and N ($EMIM^+$) in different layers. These coordination numbers were calculated accounting for i) N atoms from the first layer only, ii) N atoms from the second layer only, and iii) all N atoms regardless of their particular layer.

3.7 References

1. Georgi, N.; Kornyshev, a. a.; Fedorov, M. V., The anatomy of the double layer and capacitance in ionic liquids with anisotropic ions: Electrostriction vs. lattice saturation. *Journal of Electroanalytical Chemistry* **2010,** *649*, 261-267.

2. Vatamanu, J.; Borodin, O.; Smith, G. D., Molecular simulations of the electric double layer structure, differential capacitance, and charging kinetics for N-methyl-N-propylpyrrolidinium bis(fluorosulfonyl)imide at graphite electrodes. *The Journal of Physical Chemistry. B* **2011,** *115*, 3073-84.

3. Vatamanu, J.; Borodin, O.; Smith, G. D., Molecular insights into the potential and temperature dependences of the differential capacitance of a room-temperature ionic liquid at graphite electrodes. *Journal of the American Chemical Society.* **2010,** *132,* 14825-14833.

4. Islam, M. M. A., M. T.; Ohsaka, T., Electrical double-layer structure in ionic liquids: a corroboration of the theoretical model by experimental results. *Journal of Physical Chemistry C* **2008,** *112*, 16568-16574.

5. Lockett, V.; Horne, M.; Sedev, R.; Rodopoulos, T.; Ralston, J., Differential capacitance of the double layer at the electrode/ionic liquids interface. *Physical Chemistry Chemical Physics : PCCP* **2010,** *12*, 12499-512.

6. Su, Y.-Z.; Fu, Y.-C.; Wei, Y.-M.; Yan, J.-W.; Mao, B.-W., The electrode/ionic liquid interface: electric double layer and metal electrodeposition. *Chemphyschem : A European Journal of Chemical Physics and Physical Chemistry* **2010,** *11*, 2764-78.

CHAPTER 4

CONCLUSION

To summarize, with molecular dynamics simulations, we prove that a small change of electrode surface roughness would qualitatively change the character of the differential capacitance of EDLC. This behavior can be explained by the large differences in the structuring of ions in the electrode/electrolyte interface. Specifically, the rough surface generates an ordered pattern for ions in the double layers, but the flat surface engenders a random distribution for ions in the electric double layer.

The nonbonded potential energy, which consists of electric potential energy and intermolecular potential energy, has been calculated to explain the different rates of EDL structure change at different surfaces. According to the potential energy data, we suggest that ions are trapped at certain positions in the two layers at the flat surface, but they are easy to shift between these two layers at the rough surface. Thus, the structure changes of the electric double layer with potential are slow. Nevertheless, at the rough surface, structural changes with potential change near PZC are fast. In another word, fast structural change at low potentials means fast saturation of ion absorption at potentials near PZC, which leads to high differential capacitance according to the definition of DC. Therefore,

the fast saturation of ion absorption at the surface produces a large DC value and an overall bell-shaped DC curve. In contrast, the slow structure change of the electric double layer at the flat surface creates a small oscillation camel-shaped DC curve.

Moreover, we also found that the electrostatic interactions between ions determined the non-bonded potential energy, since the majority of the difference in potential energy between the two systems resulted from ions' electrostatic interactions. This observation is consistent with the result of coordination number, which shows that the rough surface system has more cation-anion interactions between layers while the flat surface has more of these interactions within layers. Thus, the difference of ions' electrostatic interactions leads to the difference of potential energy between the two systems. Then, the difference of potential energy generates different rates of EDL structure change at different surfaces. Finally, different rates of EDL structure change create different shapes of DC curve.

The implications of our finding are quite interesting: the specific electrolyte adsorption on the electrode surface strongly depends on the surface topology. Therefore, the crystallographic orientation and the roughness of the electrode surface can change the shape of the DC curve as a function of the electrode potential, even qualitatively. Based on the sensibly different DC curves observed for the two surfaces, we suggest that a possible route to improve the energy density of supercapacitors is to manipulate the roughness of the electrode surface.